

The Jet Composition of GRB 230307A: Poynting-Flux-Dominated Outflow?

Zhao-Wei Du,¹ HouJun Lü,^{1*} Xiaoxuan Liu¹ and EnWei Liang¹

¹Guangxi Key Laboratory for Relativistic Astrophysics, Department of Physics, Guangxi University, Nanning 530004, China;

Accepted XXX. Received YYY; in original form ZZZ

ABSTRACT

The jet composition of GRB plays an important role in understanding the energy dissipation and radiation mechanisms in GRB physics, but it is poorly constrained from the observational data. Recently, an interesting long-duration GRB 230307A with redshift $z = 0.065$ has attracted great attention. The lack of detected thermal emission and mini-structure of prompt emission lightcurve of this burst suggest that the outflow is Poynting-flux-dominated and point towards the ICMART model. In this paper, we invoke two independent methods to investigate the jet composition of GRB 230307A. The high magnetization parameter ($\sigma > 7$ or ever large) for $R_0 = 10^{10}$ cm that is used to suppress thermal component, strongly suggests that a significant fraction of the outflow energy is likely in a Poynting flux entrained with the baryonic matter. Moreover, it is found that the radiation efficiency of this burst for typical values $\epsilon_e = 0.1$ and $\epsilon_B = 0.01$ can reach as high as 50% which disfavors the internal shock model, but is consistent with ICMART model. Finally, a possible unified picture to produce GRB 230307A originated from a compact star merger is also discussed.

Key words: (stars:) gamma-ray burst: individual: GRB 230307A

1 INTRODUCTION

The observed prompt emission of Gamma-Ray burst (GRB) is believed to be from an ultra-relativistic jet, which is launched from the central engine during a catastrophic event, e.g., the core collapse of a massive star or merger of two compact stars (Kumar & Zhang 2015; Zhang 2018). Although the prompt emission of GRB was discovered much earlier than the afterglow, several open questions remain poorly to be understood in GRB physics, e.g., what is the composition of a GRB jet? How energy is dissipated to give rise to prompt emission? (Zhang 2011).

Traditionally, two scenarios of jet composition have been proposed to interpret the observations of GRB. One is matter-dominated fireball which is composed of hot photons, electron/positron pairs, and a small amount of baryons (Paczynski 1986; Goodman 1986; Shemi & Piran 1990). An initial fireball is accelerated to a relativistic speed under its own thermal pressure, and a fraction of the thermal energy is converted to the kinetic energy of the outflow (Meszaros, Laguna, & Rees 1993; Piran, Shemi, & Narayan 1993). A quasi-thermal component from the fireball photosphere should be powered when the fireball becomes transparent at the photosphere radius (photosphere model; Paczynski 1986; Goodman 1986). Moreover, a fraction of the kinetic energy of the outflow is further dissipated into heat and radiation in internal shocks to produce a non-thermal component at a larger radius (internal shock model; Rees & Meszaros 1994; Kobayashi, Piran, & Sari 1997; Daigne & Mochkovitch 1998; Pe'er, Mészáros, & Rees 2006; Zhang 2014). An alternative scenario invokes a non-thermal component from the Poynting-flux-dominated outflow where most of the energy is stored in the magnetic field.

The magnetic energy can be dissipated through magnetic reconnection or current instability to power the observed prompt emission of GRB (Thompson 1994; Lyutikov & Blandford 2003; Zhang & Pe'er 2009), or the internal-collision-induced magnetic reconnection and turbulence (ICMART) model (Zhang & Yan 2011).

From the theoretical point of view, the photosphere and internal shock models have a magnetization parameter σ much less than unity at the GRB emission site, while the ICMART model has a moderately large $\sigma > 1$ at the emission site, with the GRB emission powered by directly dissipating the magnetic energy to radiation (Zhang & Yan 2011; Gao & Zhang 2015; Chang et al. 2023). Also, the internal shock model requires a high radiation efficiency in the prompt emission (Kumar 1999; Panaitescu, Spada, & Mészáros 1999).

Observationally, (1) the quasi-thermal component predicted by the fireball model was observed in GRB 090902B (Abdo et al. 2009; Ryde et al. 2010; Pe'er et al. 2012), and it implies the matter-dominated outflow of GRB jet; (2) A good fraction of GRBs are consistent with not having a thermal component, e.g., GRB 080916C (Abdo et al. 2009; Zhang & Pe'er 2009) and GRB 130606B (Zhang et al. 2016; Oganessian et al. 2017; Rivasio et al. 2019; Burgess et al. 2020), and it suggests the Poynting-flux-dominated outflow of GRB jet; (3) A dominant non-thermal component and a sub-dominant thermal component have been discovered, e.g., GRB 100724B (Guiriec et al. 2011), GRB 110721A (Axelsson et al. 2012), GBR 160625B (Lü et al. 2017; Troja et al. 2017; Zhang et al. 2018), GRB 081221 (Hou et al. 2018), and 211211A (Chang et al. 2023), which make us believe the “hybrid” jet of GRB. In any case, the rich data observed by Fermi Gamma-Ray Burst Monitor (GBM) suggest that the GRB jet composition is likely diverse. However, it is still difficult to diagnose the jet composition of most GRBs from observational data (Zhang 2018).

* E-mail: lhj@gxu.edu.cn

Recently, an interesting long-duration GRB 230307A with redshift $z = 0.065$ that triggered the Fermi/GBM (Dalessi & Fermi GBM Team 2023), Gravitational wave high-energy Electromagnetic Counterpart All-sky Monitor (GECAM; Xiong et al. (2023)), as well as Konus-Wind (Svinkin et al. 2023), is very excited for attention and follow up observations by other telescopes (Dichiara et al. 2023; Levan et al. 2023; Yang et al. 2023; Sun et al. 2023; Yi et al. 2023). The properties of the light curve are quite similar to that of GRB 060614 (Gehrels et al. 2006), GRB 211211A (Troja et al. 2022; Rastinejad et al. 2022; Yang et al. 2022; Chang et al. 2023), and GRB 211227A (Lü et al. 2022; Ferro et al. 2023). No associated supernova signature, but a possible association with kilonova, together with heavy element nucleosynthesis, suggest that GRB 230307A originated from a binary compact star merger event (Dichiara et al. 2023; Levan et al. 2023; Yang et al. 2023; Sun et al. 2023; Yi et al. 2023). More interestingly, Yi et al. (2023) claimed that the light curve of prompt emission observed by GECAM is composed of many rapidly variable short pulses. They suggested that the jet composition is Poynting-flux-dominated and is consistent with the ICMART model.

In this paper, we invoke an independent method to investigate the jet composition of GRB 230307A. The lack of detection of a suppressed thermal component, and high magnetization parameter σ , together with high radiation efficiency, also strongly suggest a Poynting-flux-dominated jet of GRB 230307A which is consistent with the results of Yi et al. (2023). The constraints from the suppressed thermal component are presented in §2. The detail for calculating radiation efficiency is shown in §3. Conclusions are drawn in §4 with some additional discussions. Throughout the paper, we use the notation $Q = 10^n Q_n$ in CGS units and adopt a concordance cosmology with parameters $H_0 = 71 \text{ km s}^{-1} \text{ Mpc}^{-1}$, $\Omega_M = 0.30$, and $\Omega_\Lambda = 0.70$.

2 CONSTRAINTS FROM LACK OF DETECTED THERMAL EMISSION

Based on the fireball model, the emission site at which the fireball becomes transparent, is called the photosphere radius when the electron scattering optical depth ($\tau'_{\gamma e} = n' \sigma_T \Delta'$) is close to 1. Here, σ_T is the Thomson cross section, n' and Δ' are electron number density and width of the ejecta shell in the rest frame comoving with the ejecta, respectively (Mészáros & Rees 2000; Rees & Mészáros 2005; Thompson, Mészáros, & Rees 2007; Ghisellini et al. 2007; Lazzati, Morsony, & Begelman 2009). By assuming a pure baryonic flux, we derive a thermal component spectrum that can be emitted from the photosphere with a total wind luminosity of L_w (Zhang 2018). Following the method in Zhang & Pe'er (2009), the photosphere radius can be written as (Mészáros & Rees 2000; Pe'er 2008; Gao & Zhang 2015; Zhang 2018)

$$R_{\text{ph}} = \begin{cases} \left(\frac{L_w \sigma_T R_0^2}{8\pi m_p c^3 \eta} \right)^{1/3}, & R_{\text{ph}} < R_c \\ \frac{L_w \sigma_T}{8\pi m_p c^3 \Gamma^2 \eta}, & R_{\text{ph}} > R_c \end{cases} \quad (1)$$

where $\eta = L_w / \dot{M} c^2$ is dimensionless entropy of baryonic flow, $R_c \sim R_0 \times \min(\eta, \eta_*)$ is the radius where ejecta enter the 'coasting' phase, $R_0 = c \delta t^{\text{ob}}$ is the radius at which the ejecta is emitted from central engine, $\eta_* = (L_w \sigma_T / 8\pi m_p c^3 R_0)^{1/4}$ is critical dimensionless entropy, t^{ob} is the variability time scale of the central engine, m_p and c are the fundamental constants proton mass and speed of

light, respectively. The coasting Lorentz factor is $\Gamma = \eta$ and $\Gamma = \eta_*$ for $R_{\text{ph}} > R_c$ and $R_{\text{ph}} \leq R_c$, respectively.

Observed gamma-ray luminosity L_γ should be below initial wind luminosity L_w of fireball, i.e., $L_w \geq L_\gamma$. This kind of outflow contains large residual energy which may be released at the photosphere radius. So that the luminosity of the thermal component can be written as (Mészáros & Rees 2000):

$$L_{\text{th}} = \begin{cases} L_w, & \eta > \eta_*, R_{\text{ph}} < R_c \\ L_w (\eta / \eta_*)^{8/3}, & \eta < \eta_*, R_{\text{ph}} > R_c \end{cases} \quad (2)$$

One can calculate the temperature of the blackbody component which is produced from the photosphere (Mészáros & Rees 2000; Pe'er 2008),

$$T_{\text{ph}}^{\text{ob}} = \begin{cases} \left(\frac{L_w}{4\pi R_0^2 a} \right)^{1/4} (1+z)^{-1}, & R_{\text{ph}} < R_c \\ \left(\frac{L_w}{4\pi R_0^2 a} \right)^{1/4} \left(\frac{R_{\text{ph}}}{R_c} \right)^{-2/3} (1+z)^{-1}, & R_{\text{ph}} > R_c \end{cases} \quad (3)$$

where a is Stefan-Boltzman's constant.

Observationally, from soft X-rays to gamma-rays, Sun et al. (2023) performed a detailed joint-spectral analysis of the data of GRB 230307A that is observed by both GECAM and LEIA. They found that the joint spectral energy distribution (SED) can be described by power-law model, cutoff power-law model, or BAND-Cut model without thermal emission (Sun et al. 2023). Furthermore, the theoretically expected thermal peak energy is below $\sim 50 \text{ keV}$, but the photons can be heavily absorbed by column density of hydrogen below 1 keV . In order to make the coverage of energy range between 1 keV and 50 KeV , we select the spectral fitting results of the time interval for five epochs, e.g., [13-18]s, [18-25]s, [25-35]s, [35-50]s, and [50-75]s, and mark those five epochs as (a), (b), (c), (d), and (e), respectively. One interesting question is how strong of the outflow is magnetization, and it makes the lack of detection of thermal component which is suppressed.

By assuming that a pseudo blackbody spectrum is produced by the photosphere of GRB 230307A, we plot the lower limit of the expected photosphere spectrum for the internal shock model in the baryon-dominated outflow ($L_w = L_\gamma$) in Figure 1. Then, we compare it with the observational data. To ensure a clear comparison, we only plot the spectra corresponding to the epoch (a) in Figure 1. Moreover, the pseudo thermal emission depends on the radius of central engine R_0 which is poorly understood. Sun et al. (2023) reported that the minimum variability time scale of GRB 230307A is as short as $\delta t^{\text{ob}} \sim 0.01 \text{ s}$. It corresponds to radius of central engine $R_0 = 3 \times 10^8 \text{ cm}$. So, we here adopt $R_0 = 10^9 \text{ cm}$ and $R_0 = 10^{10} \text{ cm}$ to do the calculations. In the left panel of Figure 1, the red-dashed line represents a maximum temperature with $T_{\text{ph}}^{\text{ob}} = T_{\text{ph,max}}^{\text{ob}} = 28.5 \text{ keV}$ corresponding to $L_{\text{th}} = L_w$, $R_{\text{ph}} \approx R_c$, and $R_0 = 10^{10} \text{ cm}$. In order to compare, we also present two cases with lower temperatures for $T_{\text{ph}}^{\text{ob}} = 10 \text{ keV}$ and $T_{\text{ph}}^{\text{ob}} = 5 \text{ keV}$ with $\eta = 60$ and $\eta = 46$, respectively. Similar to the left panel of Figure 1, we also plot expected flux level of the photosphere emission which can be suppressed by the lower limits of magnetization parameter for different parameters within the framework of the baryonic fireball models in the right panel of Figure 1, but corresponding to $R_0 = 10^9 \text{ cm}$ and $T_{\text{ph}}^{\text{ob}} = T_{\text{ph,max}}^{\text{ob}} = 90 \text{ keV}$, as well as $T_{\text{ph}}^{\text{ob}} = 30 \text{ keV}$ and 15 keV with $\eta = 105$ and 81 , respectively.

In the left panel of Figure 1, we find that the pseudo thermal emission is significantly higher than that of observed non-thermal emission by adopting $R_0 = 10^{10} \text{ cm}$, and it is strongly in contradiction to the observed non-thermal Band-Cut component in the prompt

emission of GRB 230307A. The contradiction strongly suggests that the baryonic model at least does not work for GRB 230307A and the initial wind luminosity is not stored in the fireball form. One possible way may be to solve the above contradiction, namely, invoking a Poynting-flux-dominated outflow (Zhang & Pe'er 2009). If this is the case, the thermal emission can be suppressed (or much dimmer), and the missing luminosity as the Poynting-flux luminosity is not observable before strong magnetic dissipation at a much larger radius (Zhang & Mészáros 2002; Daigne & Mochkovitch 2002). In order to suppress the bright thermal emission, one can infer a lower limit on the magnetization parameter ($\sigma = L_p/L_b$) which is defined as the ratio between the Poynting flux (L_p) and the baryonic flux (L_b). The wind luminosity can be rewritten as $L_w = L_p + L_b = (1 + \sigma)L_b$ (Zhang & Mészáros 2002). In the derived equations of the photosphere above (Eqs. (6), (7), and (8)), the L_w can be replaced with $L_w/(1 + \sigma)$ by assuming no dissipation of the Poynting flux below R_{ph} . The precise value of σ is difficult to obtain from observational data, but one can infer the minimum value of σ which can be used to suppress (or hide) the expected thermal component from photosphere emission.

In the left panel of Figure 1, the dotted lines represent a thermal emission that makes the photosphere emission unobservable with different temperatures. It is found that the required values of σ for different temperatures at least are as high as 7, or even higher. At such high- σ , the internal shock can not power gamma-ray emission which is inconsistent with the observational data. It suggests that the internal shock model at least is not a viable mechanism to interpret GRB 230307A. So, We can confidently conclude that the ejecta of GRB 230307A is initially not in the fireball form, but is likely in a Poynting flux entrained with the baryonic matter. However, if we adopt $R_0 = 10^9$ cm, it is found that the pseudo thermal emission is higher a little bit than that of observed non-thermal emission, and it requires the $\sigma \sim 2$ which is not strongly enough to support the Poynting-flux-dominated outflow.

3 RADIATIVE EFFICIENCY OF PROMPT EMISSION

For different jet compositions of GRB, they may correspond to different energy dissipation (shocks vs. magnetic reconnection), radiation mechanisms (quasi-thermal vs. synchrotron), and dissipated radius (Rees & Meszaros 1994; Abdo et al. 2009; Ryde et al. 2010; Zhang & Pe'er 2009; Zhang & Yan 2011). The lack of detection of thermal emission of GRB 230307A implies that the photosphere model is disfavored by the energy dissipation. Theoretically, the internal shock model predicts a lower radiative efficiency (e.g., typically less than 10%; Kumar 1999; Panaitescu, Spada, & Mészáros 1999), while the ICMART model can give a relatively high efficiency (e.g., 35%~50%) by invoking a runaway generation of mini-jets (Zhang et al. 2007; Zhang & Yan 2011; Deng et al. 2015).

The GRB efficiency is defined as (Lloyd-Ronning & Zhang 2004)

$$\eta_\gamma = \frac{E_{\gamma, \text{iso}}}{E_{K, \text{iso}} + E_{\gamma, \text{iso}}} \quad (4)$$

where $E_{\gamma, \text{iso}}$ is the isotropic energy of prompt γ -ray emission, and $E_{K, \text{iso}}$ is isotropic kinetic energy. The $E_{\gamma, \text{iso}}$ is usually derived from the observed fluence (S_γ) in the detector's energy band. Due to the limited detector's energy band, we extrapolate to the rest-frame $1 \sim 10^4$ keV by using spectral parameters, called k -correction (Bloom, Frail, & Sari 2001).

$$E_{\gamma, \text{iso}} = 4\pi k d_z^2 S_\gamma (1 + z)^{-1} \quad (5)$$

where d_z is luminosity distance. Here, we adopt the spectral fitting results from GECAM (Sun et al. 2023) to do the k -correction due to the pulse pileup of saturation Fermi/GBM (Dalessi & Fermi GBM Team 2023). One has $E_{\gamma, \text{iso}} \sim 4 \times 10^{52}$ erg. The isotropic kinetic energy $E_{K, \text{iso}}$ term, on the other hand, there are two methods to estimate the value of $E_{K, \text{iso}}$. One is used to estimate it from the afterglow data through modeling which depends on the uncertain shock microphysics parameters, such as ϵ_e and ϵ_B (Freedman & Waxman 2001; Zhang et al. 2007). The other one is to directly calculate the $E_{K, \text{iso}}$ by invoking the dominant thermal spectral component and bulk Lorentz factor (Zhang, Wang, & Li 2021; Li et al. 2023). In our calculations, due to the lack of thermal emission of GRB 230307A, we adopt the first method to calculate $E_{K, \text{iso}}$ by using afterglow data.

Although the lack of detection of X-ray emission by Swift/XRT, fortunately, the Lobster Eye Imager for Astronomy (LEIA) caught the soft X-ray emission (0.5–4 keV) of this burst exactly at its trigger time (Sun et al. 2023). More interestingly, the soft X-ray light curve exhibits a plateau emission followed by a normal decay phase, namely, a smoothly broken power-law fit with decay slopes $\alpha_1 \sim 0.4$, $\alpha_2 \sim 2.33$, and break time $t_b \sim 80$ s (Sun et al. 2023). In order to calculate the $E_{K, \text{iso}}$ based on the soft X-ray emission of GRB 230307A, one needs to judge the spectral regime and environment, e.g., interstellar medium (ISM) or wind. Following the method in Zhang et al. (2006) and Lü & Zhang (2014), two independent criteria should be satisfied, namely $\alpha_1 - \alpha_2$, and the ‘closure relation’ $\alpha_2 - \beta_X$. Here β_X is the spectral index of the normal decay segment which is X-ray photon index minus 1.

Zhang & Mészáros (2001) studied energy injection from a central engine with a general luminosity law as $L(t) = L_0(t/t_0)^{-q}$, the pre-break slope α_1 should correspond to a constant energy injection from a central engine (e.g., $L(t) = L_0(t/t_0)^0$), while the post-break central engine luminosity should be $L(t) = L_0(t/t_0)^{-2}$. For the external shock model scenario, any q steeper than -2 has no effect, and it should be treated as a constant energy in the jet as $L(t) = L_0(t/t_0)^{-1}$ (Zhang et al. 2006; Gao et al. 2013). So that, the relationship can be written as

$$\alpha_1 = \begin{cases} \frac{2\alpha_2 - 3}{3}, & v_m < v < v_c \text{ (ISM)} \\ \frac{2\alpha_2 - 1}{3}, & v_m < v < v_c \text{ (Wind)} \\ \frac{2\alpha_2 - 2}{3}, & v > v_c \text{ (ISM or Wind)}. \end{cases} \quad (6)$$

Moreover, the temporal and spectral properties of the afterglow after the break (the normal decay phase) should satisfy the ‘closure relation’ of the external shock model (Zhang & Mészáros 2004; Liang, Zhang, & Zhang 2007; Gao et al. 2013)

$$\alpha_2 = \begin{cases} \frac{3\beta_X}{2} = \frac{3(p-1)}{4}, & v_m < v < v_c \text{ (ISM)} \\ \frac{3\beta_X + 1}{2} = \frac{3p-1}{4}, & v_m < v < v_c \text{ (Wind)} \\ \frac{3\beta_X - 1}{2} = \frac{3p-2}{4}, & v > v_c \text{ (ISM or Wind)} \end{cases} \quad (7)$$

Here, p is the electron's spectral distribution index. Based on the spectral fitting results from Sun et al. (2023) that is $\beta_X \sim 1.56$, one can easily judge that it should be located in the spectral regime $v_m < v < v_c$ and ISM (see Figure 2).

Based on the method in Zhang et al. (2007), the $E_{K, \text{iso}}$ can be

calculated as below in ISM with $v_m < v < v_c$,

$$E_{K,iso,52} = \left[\frac{\nu F_\nu(\nu = 10^{18} \text{Hz})}{5.2 \times 10^{-14} \text{erg s}^{-1} \text{cm}^{-2}} \right]^{4/(p+2)} \times d_{z,28}^{8/(p+2)} (1+z)^{-1} t_d^{(3p-2)/(p+2)} \times (1+Y)^{4/(p+2)} f_p^{-4/(p+2)} \epsilon_{B,-2}^{(2-p)/(p+2)} \times \epsilon_{e,-1}^{4(1-p)/(p+2)} v_{18}^{2(p-2)/(p+2)} \quad (8)$$

where $\nu F_\nu(\nu = 10^{18} \text{Hz})$ is the energy flux at 10^{18}Hz , t_d is the time in the observer frame in days. Initially, in our calculations, the microphysics parameters of the shock ϵ_e , ϵ_B , and Compton parameter Y , we adopt the typical values derived from observations $\epsilon_B = 0.01$, $\epsilon_e = 0.1$, and $Y = 1$, respectively (Panaitescu & Kumar 2002; Yost et al. 2003). However, the kinetic energy of the afterglow depends on both ϵ_e and ϵ_B , more sensitively with ϵ_e . Then, we adopt different values of $\epsilon_e = 0.1$ and 0.01 , and $\epsilon_B = 0.01, 0.001$, and 0.0001 to calculate the kinetic energy and efficiency (see Table 1). f_p is a function of the power law distribution electron spectral index p (Zhang et al. 2007)

$$f_p \sim 6.73 \left(\frac{p-2}{p-1} \right)^{p-1} (3.3 \times 10^{-6})^{(p-2.3)/2} \quad (9)$$

After deriving both $E_{\gamma,iso}$ and $E_{k,iso}$, one can calculate the radiative efficiency for different ϵ_e and ϵ_B , and the results are shown in Table 1. More interestingly, it is found that the radiative efficiency η_γ is as high as 50% of GRB 230307A for $\epsilon_e = 0.1$ and $\epsilon_B = 0.01$. It is significantly higher than the typical efficiency of the internal shock scenario, but is consistent with that of expected by ICMART with a Poynting-flux-dominated jet. This is also consistent with that of results from Yi et al. (2023) based on the mini-structure of the prompt emission lightcurve to claim the ICMART model a Poynting-flux-dominated outflow.

4 CONCLUSION AND DISCUSSION

In this paper, we investigate the jet composition of GRB 230307A by invoking two independent methods. First, the lack of detection of thermal emission expected from the baryonic model provides strong evidence to constrain the composition of the fireball: the outflow of GRB 230307A should be Poynting-flux-dominated with a magnetization parameter ($\sigma > 7$) at the photosphere in order to suppress thermal component and account for the observed spectra for $R_0 = 10^{10} \text{cm}$ (see Figure 1). It suggests that a significant fraction of the Poynting flux energy is not likely to be directly converted to the kinetic energy of the outflow below the photosphere. Second, the radiative efficiency $\eta_\gamma \sim 50\%$ of GRB 230307A for $\epsilon_e = 0.1$ and $\epsilon_B = 0.01$, is significantly higher than the typical efficiency of the internal shock scenario, but is consistent with that of expected by ICMART with a Poynting-flux-dominated jet.

In our calculations, first, we only account for epoch (a) with the brightest one to present the pseudo thermal emission and calculate the minimum values of σ for different temperatures. Moreover, we also attempt to apply for epochs (b), (c), (d), and (e), and find that the peak of the thermal component still exceeds the observed data. It still requires that a minimum of σ is as high as 5 (or 4, 4, and 3) for epoch (b) (or (c), (d), and (e)) with different temperatures at $R_0 = 10^{10} \text{cm}$. It means that at least 83% (or 80%, 80%, and 75%) of the energy is stored in the form of Poynting flux for epoch (b) (or (c), (d), and (e)) even considering the evolution of jet composition during such short time-scale. Second, the calculated efficiency is dependent

on the microphysical parameters of the shock, namely ϵ_e and ϵ_B which are poorly constrained from the observational data. The high efficiency $\eta_\gamma \sim 50\%$ for typical values of $\epsilon_e = 0.1$ and $\epsilon_B = 0.01$, at least tell us the possible of existing high efficiency that is consistent with Poynting-flux-dominated outflow.

In any case, the lack of detection of thermal emission required a high magnetization parameter, together with a high radiation efficiency, strongly suggest that a significant fraction of the outflow energy is likely in a Poynting flux entrained with the baryonic matter rather than a pure baryonic flux. It is consistent with that of results from Yi et al. (2023) who claimed a Poynting-flux-dominated outflow with ICMART model based on the mini-structure of prompt emission lightcurve of this burst.

Based on the previous studies and some observational clues of GRB 230307A, e.g., lack of supernova-associated, but associated with a possible kilonova emission, the heavy element nucleosynthesis, and the characteristic of soft X-ray emission (Dichiara et al. 2023; Levan et al. 2023; Yang et al. 2023; Sun et al. 2023; Yi et al. 2023), point towards a compact star merger origin, and a unified picture can be accounted for as follows. The central engine of GRB 230307A is a millisecond magnetar which is the post-merger product of NS-NS mergers (supported by a lanthanide-rich kilonova). It can launch a relativistic jet via energy extraction mechanisms, such as spin-down, magnetic bubble eruption due to differential rotation, or accretion (Zhang 2018). The observed bright gamma-ray emission can be powered by dissipation of the Poynting flux energy via synchrotron radiation. The extra soft X-ray plateau component detected by LEIA (Sun et al. 2023) can be powered by magnetic dipole spin-down of magnetar. Finally, the shocks interact with the interstellar medium to produce the observed multi-wavelength afterglow emission. However, we can not completely rule out the NS-BH merger (or NS-NS merger) with the BH central engine.

ACKNOWLEDGEMENTS

This work is supported by the Guangxi Science Foundation the National (grant Nos. 2023GXNSFDA026007, and 2017GXNSFFA198008), the Natural Science Foundation of China (grant Nos. 11922301 and 12133003), and the Program of Bagui Scholars Program (LHJ).

DATA AVAILABILITY

This is the theoretical work, and there are no new data associated with this article.

REFERENCES

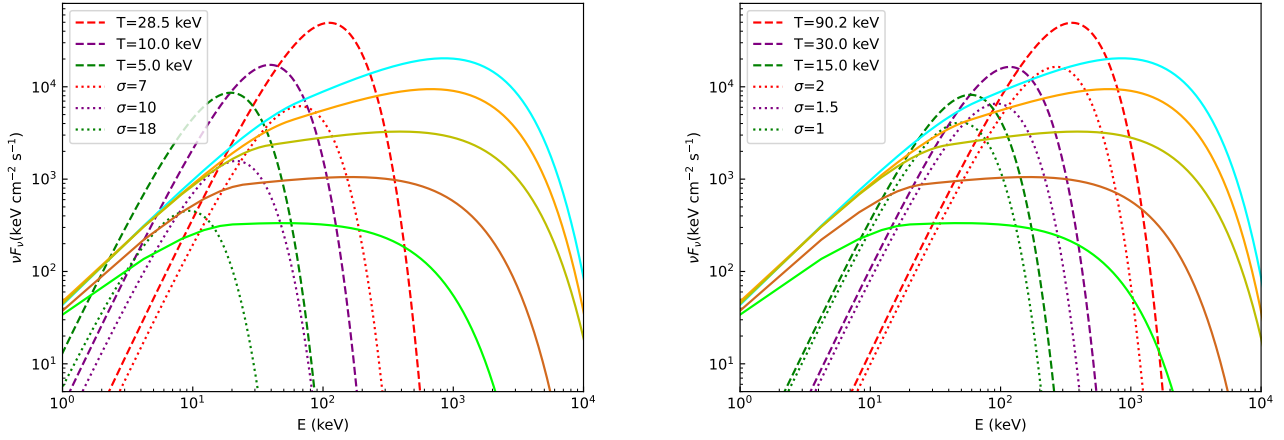
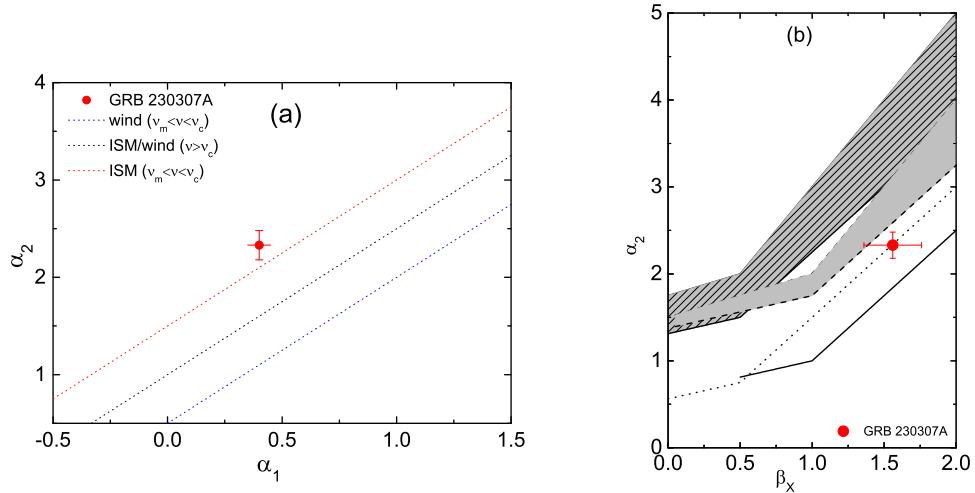
- Abdo A. A., Ackermann M., Ajello M., Asano K., Atwood W. B., Axelsson M., Baldini L., et al., 2009, *ApJL*, 706, L138. doi:10.1088/0004-637X/706/1/L138
- Abdo A. A., Ackermann M., Arimoto M., Asano K., Atwood W. B., Axelsson M., Baldini L., et al., 2009, *Sci*, 323, 1688. doi:10.1126/science.1169101
- Axelsson M., Baldini L., Barbiellini G., Baring M. G., Bellazzini R., Bregeon J., Brigida M., et al., 2012, *ApJL*, 757, L31. doi:10.1088/2041-8205/757/2/L31
- Bloom J. S., Frail D. A., Sari R., 2001, *AJ*, 121, 2879. doi:10.1086/321093
- Burgess J. M., Bégué D., Greiner J., Giannios D., Bachelj A., Berlato F., 2020, *NatAs*, 4, 174. doi:10.1038/s41550-019-0911-z
- Chang X.-Z., Lü H.-J., Yang X., Chen J.-M., Liang E.-W., 2023, *ApJ*, 943, 146. doi:10.3847/1538-4357/aca969

- Daigne F., Mochkovitch R., 2002, *A&A*, 388, 189. doi:10.1051/0004-6361:20020415
- Daigne F., Mochkovitch R., 1998, *MNRAS*, 296, 275. doi:10.1046/j.1365-8711.1998.01305.x
- Dalessi S., Fermi GBM Team, 2023, *GCN*, 33407, 1
- Deng W., Li H., Zhang B., Li S., 2015, *ApJ*, 805, 163. doi:10.1088/0004-637X/805/2/163
- Dichiara S., Tsang D., Troja E., Neill D., Norris J. P., Yang Y.-H., 2023, *ApJL*, 954, L29. doi:10.3847/2041-8213/acf21d
- Ferro M., Brivio R., D'Avanzo P., Rossi A., Izzo L., Campana S., Christensen L., et al., 2023, *A&A*, 678, A142. doi:10.1051/0004-6361/202347113
- Freedman D. L., Waxman E., 2001, *ApJ*, 547, 922. doi:10.1086/318386
- Gao H., Zhang B., 2015, *ApJ*, 801, 103. doi:10.1088/0004-637X/801/2/103
- Gao H., Lei W.-H., Zou Y.-C., Wu X.-F., Zhang B., 2013, *NewAR*, 57, 141. doi:10.1016/j.newar.2013.10.001
- Gehrels N., Norris J. P., Barthelmy S. D., Granot J., Kaneko Y., Kouveliotou C., Markwardt C. B., et al., 2006, *Natur*, 444, 1044. doi:10.1038/nature05376
- Ghisellini G., Celotti A., Ghirlanda G., Firmani C., Nava L., 2007, *MNRAS*, 382, L72. doi:10.1111/j.1745-3933.2007.00392.x
- Goodman J., 1986, *ApJL*, 308, L47. doi:10.1086/184741
- Guiriec S., Connaughton V., Briggs M. S., Burgess M., Ryde F., Daigne F., Mészáros P., et al., 2011, *ApJL*, 727, L33. doi:10.1088/2041-8205/727/2/L33
- Hou S.-J., Zhang B.-B., Meng Y.-Z., Wu X.-F., Liang E.-W., Lü H.-J., Liu T., et al., 2018, *ApJ*, 866, 13. doi:10.3847/1538-4357/aadc07
- Kobayashi S., Piran T., Sari R., 1997, *ApJ*, 490, 92. doi:10.1086/512791
- Kumar P., 1999, *ApJL*, 523, L113. doi:10.1086/312265
- Kumar P., Zhang B., 2015, *PhR*, 561, 1. doi:10.1016/j.physrep.2014.09.008
- Lazzati D., Morsony B. J., Begelman M. C., 2009, *ApJL*, 700, L47. doi:10.1088/0004-637X/700/1/L47
- Levan A., Gompertz B. P., Salafia O. S., Bulla M., Burns E., Hotokezaka K., Izzo L., et al., 2023, *arXiv*, arXiv:2307.02098. doi:10.48550/arXiv.2307.02098
- Li L., Wang Y., Ryde F., Pe'er A., Zhang B., Guiriec S., Castro-Tirado A. J., et al., 2023, *ApJL*, 944, L57. doi:10.3847/2041-8213/acb99d
- Liang E.-W., Zhang B.-B., Zhang B., 2007, *ApJ*, 670, 565. doi:10.1086/521870
- Lloyd-Ronning N. M., Zhang B., 2004, *ApJ*, 613, 477. doi:10.1086/423026
- Lyutikov M., Blandford R., 2003, *arXiv*, astro-ph/0312347. doi:10.48550/arXiv.astro-ph/0312347
- Lü H.-J., Yuan H.-Y., Yi T.-F., Wang X.-G., Hu Y.-D., Yuan Y., Rice J., et al., 2022, *ApJL*, 931, L23. doi:10.3847/2041-8213/ac6e3a
- Lü H.-J., Lü J., Zhong S.-Q., Huang X.-L., Zhang H.-M., Lan L., Xie W., et al., 2017, *ApJ*, 849, 71. doi:10.3847/1538-4357/aa8f99
- Lü H.-J., Zhang B., 2014, *ApJ*, 785, 74. doi:10.1088/0004-637X/785/1/74
- Mészáros P., Laguna P., Rees M. J., 1993, *ApJ*, 415, 181. doi:10.1086/173154
- Mészáros P., Rees M. J., 2000, *ApJ*, 530, 292. doi:10.1086/308371
- Oganesyan G., Nava L., Ghirlanda G., Celotti A., 2017, *ApJ*, 846, 137. doi:10.3847/1538-4357/aa831e
- Paczynski B., 1986, *ApJL*, 308, L43. doi:10.1086/184740
- Panaiteescu A., Spada M., Mészáros P., 1999, *ApJL*, 522, L105. doi:10.1086/312230
- Panaiteescu A., Kumar P., 2002, *ApJ*, 571, 779. doi:10.1086/340094
- Pe'er A., Zhang B.-B., Ryde F., McGlynn S., Zhang B., Preece R. D., Kouveliotou C., 2012, *MNRAS*, 420, 468. doi:10.1111/j.1365-2966.2011.20052.x
- Pe'er A., 2008, *ApJ*, 682, 463. doi:10.1086/588136
- Pe'er A., Mészáros P., Rees M. J., 2006, *ApJ*, 642, 995. doi:10.1086/501424
- Piran T., Shemi A., Narayan R., 1993, *MNRAS*, 263, 861. doi:10.1093/mnras/263.4.861
- Rastinejad J. C., Gompertz B. P., Levan A. J., Fong W.-fai., Nicholl M., Lamb G. P., Malesani D. B., et al., 2022, *Natur*, 612, 223. doi:10.1038/s41586-022-05390-w
- Ravasio M. E., Ghirlanda G., Nava L., Ghisellini G., 2019, *A&A*, 625, A60. doi:10.1051/0004-6361/201834987
- Rees M. J., Meszaros P., 1994, *ApJL*, 430, L93. doi:10.1086/187446
- Rees M. J., Mészáros P., 2005, *ApJ*, 628, 847. doi:10.1086/430818
- Ryde F., Axelsson M., Zhang B. B., McGlynn S., Pe'er A., Lundman C., Larson S., et al., 2010, *ApJL*, 709, L172. doi:10.1088/2041-8205/709/2/L172
- Shemi A., Piran T., 1990, *ApJL*, 365, L55. doi:10.1086/185887
- Sun H., Wang C.-W., Yang J., Zhang B.-B., Xiong S.-L., Yin Y.-H. I., Liu Y., et al., 2023, *arXiv*, arXiv:2307.05689. doi:10.48550/arXiv.2307.05689
- Svinkin D., Frederiks D., Ulanov M., Tsvetkova A., Lysenko A., Ridnaia A., Cline T., et al., 2023, *GCN*, 33427, 1
- Thompson C., Mészáros P., Rees M. J., 2007, *ApJ*, 666, 1012. doi:10.1086/518551
- Thompson C., 1994, *MNRAS*, 270, 480. doi:10.1093/mnras/270.3.480
- Troja E., Lipunov V. M., Mundell C. G., Butler N. R., Watson A. M., Kobayashi S., Cenko S. B., et al., 2017, *Natur*, 547, 425. doi:10.1038/nature23289
- Troja E., Fryer, C. L., O'Connor, B., et al. 2022, *Nature*, 612, 228. doi:10.1038/s41586-022-05327-3
- Xiong S., Wang C., Huang Y., Gecam Team, 2023, *GCN*, 33406
- Yang J., Ai S., Zhang B.-B., Zhang B., Liu Z.-K., Wang X. I., Yang Y.-H., et al., 2022, *Natur*, 612, 232. doi:10.1038/s41586-022-05403-8
- Yang Y.-H., Troja E., O'Connor B., Fryer C. L., Im M., Durbak J., Paek G. S. H., et al., 2023, *arXiv*, arXiv:2308.00638. doi:10.48550/arXiv.2308.00638
- Yi S.-X., Wang C.-W., Zhang B., Xiong S.-L., Zhang S.-N., Tan W.-J., Liu J.-C., et al., 2023, *arXiv*, arXiv:2310.07205. doi:10.48550/arXiv.2310.07205
- Yost S. A., Harrison F. A., Sari R., Frail D. A., 2003, *ApJ*, 597, 459. doi:10.1086/378288
- Zhang B.-B., Zhang B., Castro-Tirado A. J., Dai Z. G., Tam P.-H. T., Wang X.-Y., Hu Y.-D., et al., 2018, *NatAs*, 2, 69. doi:10.1038/s41550-017-0309-8
- Zhang B.-B., Uhm Z. L., Connaughton V., Briggs M. S., Zhang B., 2016, *ApJ*, 816, 72. doi:10.3847/0004-637X/816/2/72
- Zhang B., Mészáros P., 2002, *ApJ*, 581, 1236. doi:10.1086/344338
- Zhang B., 2014, *IJMPD*, 23, 1430002. doi:10.1142/S021827181430002X
- Zhang B., 2011, *CRPhy*, 12, 206. doi:10.1016/j.crhy.2011.03.004
- Zhang B., Wang Y., Li L., 2021, *ApJL*, 909, L3. doi:10.3847/2041-8213/abe6ab
- Zhang B., 2018, *pgrb.book*. doi:10.1017/9781139226530
- Zhang B., Liang E., Page K. L., Grupe D., Zhang B.-B., Barthelmy S. D., Burrows D. N., et al., 2007, *ApJ*, 655, 989. doi:10.1086/510110
- Zhang B., Fan Y. Z., Dyks J., Kobayashi S., Mészáros P., Burrows D. N., Nousek J. A., et al., 2006, *ApJ*, 642, 354. doi:10.1086/500723
- Zhang B., Pe'er A., 2009, *ApJL*, 700, L65. doi:10.1088/0004-637X/700/2/L65
- Zhang B., Mészáros P., 2004, *IJMPA*, 19, 2385. doi:10.1142/S0217751X0401746X
- Zhang B., Yan H., 2011, *ApJ*, 726, 90. doi:10.1088/0004-637X/726/2/90
- Zhang B., Mészáros P., 2001, *ApJL*, 552, L35. doi:10.1086/320255

This paper has been typeset from a $\text{\TeX}/\text{\LaTeX}$ file prepared by the author.

Table 1. Radioactive efficiency for different values of ϵ_B and ϵ_e .

ϵ_e	ϵ_B	η_γ
0.1	0.01	50.7%
0.1	0.001	31.66%
0.1	0.0001	17.26%
0.01	0.01	0.93%
0.01	0.001	0.42%
0.01	0.0001	0.19%

**Figure 1.** Left: The observed Band-cut spectra for five epochs (taken from Sun et al. (2023)) and the predicted lower limits of the photosphere spectra (dashed lines) for different temperatures with $R_0 = 10^{10}$ cm by adopting the epoch (a) within the framework of the baryonic fireball models. The dotted lines represent a thermal emission that makes the photosphere emission unobservable with different temperatures. Right: Similar to the left panel, but for different temperatures with $R_0 = 10^9$ cm.**Figure 2.** (a): Relationships between temporal decay indices α_1 and α_2 in different spectral regions and environments. The three solid lines indicate the closure relations of three specific external shock models invoking a constant energy injection. (b): Temporal decay index α_2 against spectral index β_X along with the closure relations of the external shock model in the case of ISM. The solid line (pre-jet break) and the shaded region (post jet break) are for the spectral regime I ($\nu > \max(\nu_c, \nu_m)$), while the dashed line (pre-jet break) and hatched region (post jet break) are for the spectral regime II ($\nu_m < \nu < \nu_c$).